Influence of rotational excitation and collision energy on the stereo dynamics of the reaction: $N(^4S)+H_2$ $(v = 0, j = 0, 2, 5, 10)\rightarrow NH(X^3\Sigma^-)+H^*$

Yu Yong-Jiang(于永江)†, Xu Qiang(徐 强), and Xu Xiu-Wei(徐秀玮)

School of Physics, Ludong University, Yantai 264025, *China*

(Received 29 May 2011; revised manuscript received 26 June 2011)

The N+H_2 reaction has attracted a great deal of attention from both the experimental and the theoretical community, and most of the attention has been paid to the first excited state N(^{2}D) atoms in collisions with hydrogen molecules and the scalar properties of the reaction. In this paper, we study the stereo dynamical properties and calculate the reaction cross sections of the N(^{4}S) + H_2 (v=0, j=0, 2, 5, 10) → NH($X^3\Sigma^-$) + H using the quasi-classical trajectory (QCT) method on an accurate NH_2 potential energy surface (PES) reported by Poveda and Varandas [Poveda L A and Varandas A J C 2005 *Phys. Chem. Chem. Phys.* **7** 2867], in a collision energy range of 25 kcal·mol^{-1}–140 kcal·mol^{-1}. Results indicate that the reactant rotational excitation and initial collision energy both have a considerable influence on the distributions of the $\boldsymbol{k}$–$\boldsymbol{j}'$ correlation, the $\boldsymbol{k}$–$\boldsymbol{k}'$–$\boldsymbol{j}'$ correlation and $\boldsymbol{k}$–$\boldsymbol{k}'$ correlation. The differential cross section is found to be sensitive to collision energy.

Keywords: quasi-classical trajectory method, vector correlation, differential cross section

PACS: 34.50.Lf, 82.20.Kh **DOI:** 10.1088/1674-1056/20/12/123402

1. Introduction

The N+H_2 reaction plays an important role in atmospheric chemistry and combustion chemistry.[1,2] The N+H_2 reaction, for instance, is a very important reaction in the thermal decompositions of $C_3H_6N_6O_6$ and $C_4H_8N_8O_8$, which are important ingredients in solid propellants for rockets and guns.[3] It has attracted a great deal of attention from both experimental and theoretical communities, with most of the attention has been paid to the first excited state N(^{2}D) atoms in collisions with hydrogen molecules[4–8] due to less reactivity of the ground state of atomic nitrogen N(^{4}S). Additionally, the reaction N(^{4}S) + H_2 → NH($X^3\Sigma^-$) + H is also very interesting as the simplest bimolecular reaction of N atoms. However, there have been few direct experimental and theoretical studies on this topic so far.

Experimentally, Koshi *et al.*[9] investigated the reactions of N(^{4}S) atoms with NO and H_2 through the direct detection of N atoms by the atomic resonance absorption technique in a shock tube apparatus and the rate constant of the reaction N(^{4}S) + H_2 → NH + H has been determined by adding H_2 into the NO–Ar mixture, with $k = (2.8 \pm 0.2) \times 10^{14} \exp(-E_a/RT)$ (cm^3·mol^{-1}·s^{-1}), where $E_a = (33 \pm 7)$ kcal·mol^{-1}. In order to ascertain the mechanism of this reaction, a quantum mechanical calculation was performed and the results suggested that the reaction N (^{4}S) + H_2 → NH + H proceeds via a direct abstraction of H atom from H_2, and the calculated activation energy is in good agreement with the experimental result.[9] Theoretically, Takayanagi *et al.*[10] calculated the potential energy surfaces (PES) for the N(^{4}S, ^{2}D, ^{2}P) + H_2 reactions using the *ab initio* multireference configuration interaction method, in which two-dimensional surfaces were constructed for collinear and perpendicular approaches of N + H_2 in order to understand the mechanisms of these reactions. The calculations predicted that both the lowest and the second lowest doublet surfaces contribute to the reaction dynamics of N(^{2}D) + H_2, and the two surfaces intersect with the lowest quartet surface of N(^{4}S) + H_2 in the intermediate region. Using a direct *ab initio* dynamics method, Zhang and Thanh[11] studied the potential energy surface of the title reaction for low electronic states at the QCISD/cc-p VDZ level of theory and it was found that the ground-state reaction is N(^{4}S) + H_2 → NH($^3\Sigma^-$) + H. Pas-

*Project supported by the Natural Science Foundation of Shandong Province of China (Grant No. Z2008A02).

†Corresponding author. E-mail: ldyuyongjiang@yahoo.com.cn

© 2011 Chinese Physical Society and IOP Publishing Ltd

cual *et al.*[12] performed the calculations by using the quasi-classical trajectory (QCT) and transition state theory method (TST) on their own PES, and the rate constants for the forward and reverse reactions were found to be in good accordance with available experimental[9,13] and theoretical data.[11] In 2005, Poveda and Varandas[14] reported on a highly accurate PES[14] for the quartet state of NH_2 through the *ab initio* calculations with the multi-reference configuration interaction method,[15,16] in which the calculations involved seven correlated electrons in six active orbits, amounting to a total of 50 configuration state functions. The calculated raw *ab initio* energies were then corrected semi-empirically by the double many-body expansion (DMBE) theory.[17] Their corrected energies were subsequently examined and compared carefully with the results from previous studies on the title system, showing good agreement with the experimental data and the best theoretical estimates available. Han *et al.*[18] investigated the reaction $H(^2S)$ + NH→ $N(^4S)$ + H_2 by quasi-classical trajectory (QCT) and quantum mechanics on the DMBE PES,[14] and the results accorded with the experimental data.[19]

Most of the previous studies in reaction dynamics have focused on scalar properties, such as the rate constant, cross section and product population distribution. However, complete information about the forces in the reaction also needs to consider vector properties, such as velocities and angular momentum, for they possess not only magnitudes that can be directly related to translational and rotational energies, but also well-defined directions.[20,21] Hence, a complete understanding of the gas-phase reaction dynamics is possible only after both scalar and vector properties have been taken into account.[21,22] Theoretical and experimental interest in vector correlation of the three-atoms reaction have increased significantly in recent decades.[23−26] It is well recognized that product rotational polarization can provide the detailed mechanistic information.[27,28] However, to the best of our knowledge, there is no study of vector correlation (the so-called stereo dynamics) for the influence of the rotational effect on the DMBE PES[14] so far. In the present study, to probe the title reaction, we perform the QCT calculations on the DMBE PES[14] so as to study the stereo dynamics of the reaction $N(^4S)$ + H_2 (v = 0, j = 0, 2, 5, 10) → $NH(X^3\Sigma^-)$ + H, which occurs on the ground state PES, and some interesting results are found. This paper is organized as follows: In Section 2, a brief description of the theoretical methods and computational details are presented. Then the results and the discussion are given in Section 3. Finally, conclusions are summarized in Section 4.

2. Theory

2.1. Rotational polarization of product

The centre-of-mass (CM) reference frame is used in the calculation as shown in Fig. 1. The z axis is parallel to the initial relative velocity vector $\boldsymbol{k}$ whereas the y axis is perpendicular to the x–z plane containing the initial and the final relative velocity vectors, $\boldsymbol{k}$ and $\boldsymbol{k}'$. θ_t is the scattering angle between $\boldsymbol{k}$ and $\boldsymbol{k}'$. θ_r and ϕ_r are the polar and azimuthal angles of the final rotational angular momentum $\boldsymbol{j}'$. The full three-dimensional angular distribution associated with $\boldsymbol{k}$, $\boldsymbol{k}'$ and $\boldsymbol{j}'$ can be represented by a set of generalized polarization-dependent differential cross sections (PDDCSs) in the CM frame.[29,30] The fully correlated CM angular distribution is written as the sum

$$P(\omega_t, \omega_r) = \sum_{kq} \frac{[k]}{4\pi} \frac{1}{\sigma} \frac{\mathrm{d}\sigma_{kq}}{\mathrm{d}\omega_t} C_{kq}(\omega_r), \qquad (1)$$

where $[k] = 2k + 1$. The angles $\omega_t = \theta_t$, ϕ_t, and $\omega_r = \theta_r$, ϕ_r refer to the coordinates of the unit vectors $\boldsymbol{k}'$ and $\boldsymbol{j}'$ along the directions of the product relative velocity and angular momentum vectors in the CM frame, respectively. σ represents the integral cross section and $(1/\sigma)(\mathrm{d}\sigma_{kq}/\mathrm{d}\omega_t)$ denotes the PDDCS. $C_{kq}(\omega_r)$ is a modified spherical harmonics.

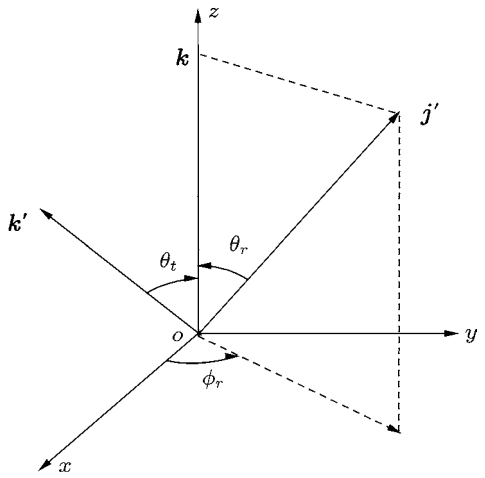


Fig. 1. Centre-of-mass coordinate system used to describe the correlations between $\boldsymbol{k}$, $\boldsymbol{k}'$, and $\boldsymbol{j}'$.

The distribution function $P(\theta_r)$ describing the $\boldsymbol{k}$–$\boldsymbol{j}'$ correlation can be expanded in a series of Legendre

polynomials as[21,31−33]

$$P(\theta_r) = \frac{1}{2}\sum_k (2k+1)a_0^{(k)}\mathrm{P}_k(\cos\theta_r). \quad (2)$$

In this paper, $P(\theta_r)$ is expanded up to $k = 18$, which shows good convergence, and

$$\begin{aligned} a_0^{(k)} &= \int_0^{\pi} P(\theta_r)\mathrm{P}_k(\cos\theta_r)\sin\theta_r \,\mathrm{d}\theta_r \\ &= \langle \mathrm{P}_k(\cos\theta_r)\rangle . \end{aligned} \quad (3)$$

The expanding coefficient $a_0^{(k)}$ is called orientation parameter (when k is odd) or alignment parameter (when k is even). Specially, when $k = 2$, it indicates the product rotational alignment[34] and is expressed as

$$\begin{aligned} a_0^2 &= \langle \mathrm{P}_2(\cos\theta_r)\rangle = \langle \mathrm{P}_2(\boldsymbol{j}'\cdot\boldsymbol{k})\rangle \\ &= \frac{1}{2}\left\langle 3\cos^2\theta_r - 1\right\rangle . \end{aligned} \quad (4)$$

Since the rotational alignment of the product has been measured in most experiments, we only calculate the average rotational alignment factor $\langle \mathrm{P}_2(\cos\theta_r)\rangle$ in this work.

The dihedral angle distribution function $P(\phi_r)$ describing $\boldsymbol{k}$–$\boldsymbol{k}'$–$\boldsymbol{j}'$ correlation can be expanded in Fourier series as

$$\begin{aligned} P(\phi_r) = \frac{1}{2\pi}\Bigg(1 &+ \sum_{\mathrm{even},n\geq 2} a_n\cos n\phi_r \\ &+ \sum_{\mathrm{odd},n\geq 1} b_n \sin n\phi_r\Bigg), \end{aligned} \quad (5)$$

where $a_n = 2\langle\cos n\phi_r\rangle$ and $b_n = 2\langle\sin n\phi_r\rangle$. In the present calculations, $P(\phi_r)$ is expanded up to $n = 24$ for a good convergence.

2.2. Potential energy surface properties

The major feature of the present quartet surface is the N–H–H collinear transition state for reaction $\mathrm{N}(^4\mathrm{S}) + \mathrm{H}_2\ (\mathrm{X}^1\Sigma_g^+) \rightarrow \mathrm{NH}\ (\mathrm{X}^3\Sigma^-) + \mathrm{H}(^2\mathrm{S})$, which is highlighted in Fig. 2(a). Contours are equally spaced by 10 kcal·mol^{-1}. The PES has a saddle point with the coordinates at (1.17 Å, 1.12 Å, 1 Å=0.1 nm). The reaction profile along the minimum energy path from reactants to products on our selected PES is shown in Fig. 2(b). Forward barrier height of the reaction is about 28 kcal·mol^{-1}, which is close to the experimental values,[9,13] thus indicating the reaction is an endothermic reaction.

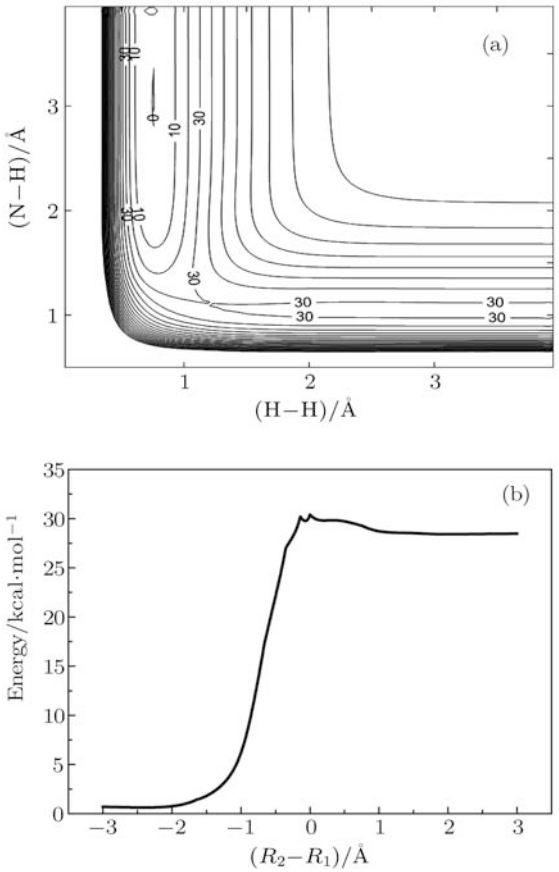


Fig. 2. Potential energy surfaces, showing (a) contours for stretching of N–H–H in linear configurations, and (b) reaction profile along the minimum energy path from the reactants to the products on our chosen PES of the N + H_2 reaction.

2.3. Quasi-classical trajectory calculations

We employ the standard quasi-classical trajectory (QCT) method[35−40] to study the stereo dynamics of the reaction $\mathrm{N}(^4\mathrm{S}) + \mathrm{H}_2$ ($v = 0$, $j = 0$, 2, 5, 10) $\rightarrow \mathrm{NH}(\mathrm{X}^3\Sigma^-) + \mathrm{H}$. In the calculation, the resonance effect and the tunneling effect are ignored, and the current reaction is considered as an adiabatic process. Therefore, the QCT treatment of the title reaction is sufficiently accurate. In the calculations, the classical Hamilton equation is numerically integrated in three dimensions and the accuracy of the integration is verified by checking the conservations of total energy and total angular momentum for each trajectory. The vibrational and the rotational levels of the reactant molecules are taken to be $v = 0$ and $j = 0$, 2, 5, 10, respectively. The values of selected collision energy (E_c) for the reaction are in a range from 25 kcal·mol^{-1} to 140 kcal·mol^{-1} in steps of 5 kcal·mol^{-1}. For the reaction threshold energy of interest, the reactions of

collision energies less than 30 kcal·mol^{-1} are investigated carefully. Batches of total 10×10^5 trajectories are run for each collision energy. The integration step size is 0.1 fs and the trajectories are started at an initial distance of 15 Å between the N atom and the centre of mass of the H_2 molecule.

3. Results and discussion

The energy dependence of the integral reaction cross section (ICS) for the ground internal state of H_2 ($v = 0$, $j = 0$) is displayed in Fig. 3 for collision energy (E_c) in the range of 25 kcal·mol^{-1}–140 kcal·mol^{-1}, which shows that the ICS is in good agreement with the results calculated by Pascual *et al.*[12] It can be seen clearly that the ICS increases quickly with the increase of the collision energy in a range from 25 kcal·mol^{-1} to 75 kcal·mol^{-1}, while the increase of ICS slows down when the collision energy is higher than 75 kcal·mol^{-1} and the maximum is obtained when the collision energy reaches about 110 kcal·mol^{-1}. The reaction threshold energy is about 25 kcal·mol^{-1} due to the entrance channel potential barrier, which accords well with the forward barrier of the ground-state reaction which was reported to be 26.9 kcal·mol^{-1} in theory[14] and 25.1 kcal·mol^{-1} in experiment.[13] Unlike most barrierless insertion reactions whose cross sections decay monotonically with energy,[41] the cross section of the title reaction increases monotonically with energy due to the threshold, demonstrating that it is a reaction of abstraction.

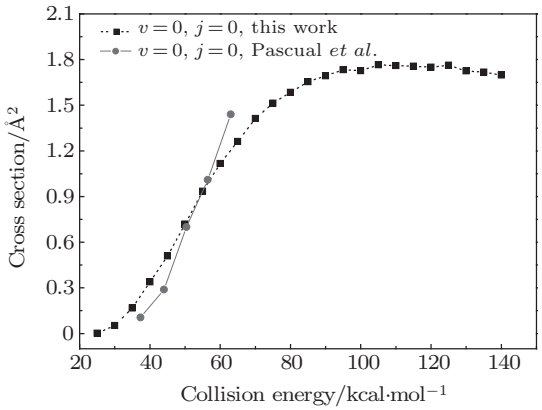


Fig. 3. Energy dependences of initial state-specified ($v = 0$ and $j = 0$) integral cross section for the N + H_2 reaction on the PES of the present and the cited work.

The $P(\theta_r)$ distribution of the product NH describes the $\boldsymbol{k}$–$\boldsymbol{j}'$ correlation. The calculated distributions of $P(\theta_r)$ for three collision energies (E_c = 35, 75 and 115 kcal·mol^{-1}) with the vibrational ground state and four different rotational quantum states on the PES are shown in Figs. 4(a), 4(b) and 4(c) respectively. Apparently, there is an obvious discrepancy between the distributions of $P(\theta_r)$ with different values of rotational quantum number for all collision energies. The peaks of $P(\theta_r)$ are located at $\theta_r = 90°$ and symmetric with respect to $\theta = 90°$ in

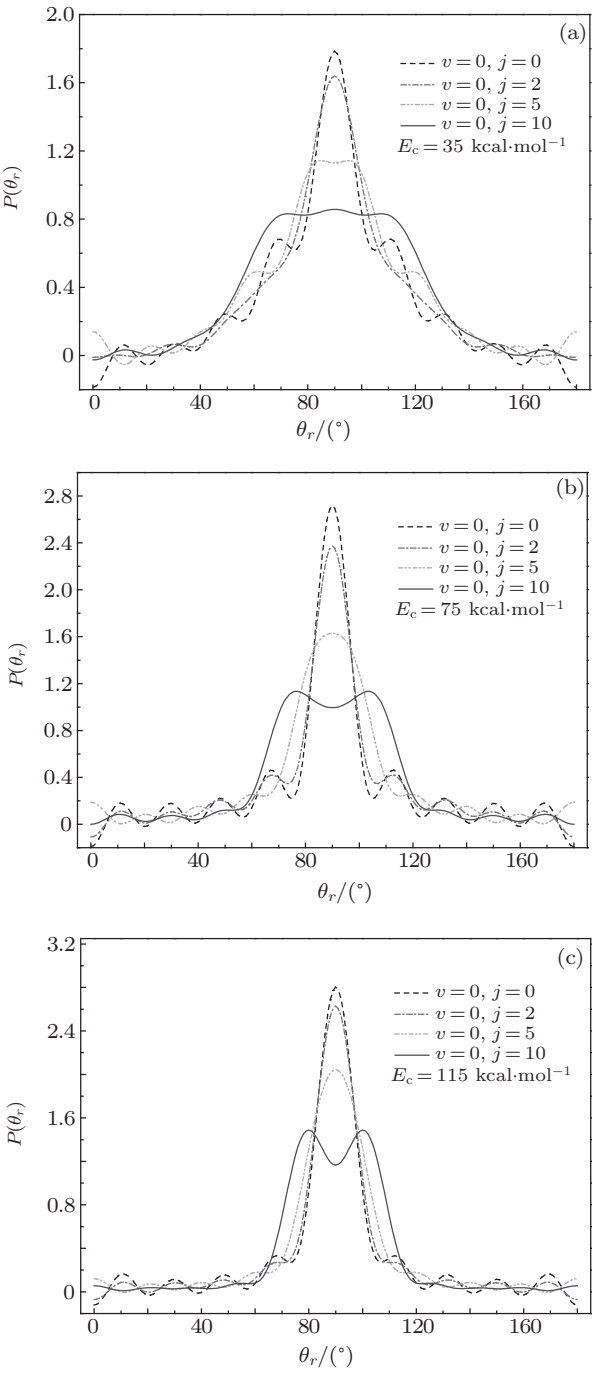


Fig. 4. Angular distributions of $P(\theta_r)$ on the PES at three collision energies reflecting the $\boldsymbol{k}$–$\boldsymbol{j}'$ correlation at E_c = 35 kcal·mol^{-1} (a), 75 kcal·mol^{-1} (b), and 110 kcal·mol^{-1} (c).

the cases of $j = 0$ and $j = 2$ for all collision energies, which shows that the product rotational angular momentum vector is strongly aligned along the direction perpendicular to the relative velocity direction. The peak of $P(\theta_r)$ becomes broader and lower as rotational quantum state increases. The $P(\theta_r)$ distribution displays a distinct V-shaped splitting around $\theta_r = 90^\circ$ when $j = 5$ at $E_c = 35$ kcal·mol^{-1}, $j = 10$ at $E_c = 75$ kcal·mol^{-1}, and $j = 10$ at $E_c = 115$ kcal·mol^{-1} as indicated in Figs. 4(a), 4(b) and 4(c) separately. In the case of a certain collision energy, the larger the value of a rotational quantum number is, the lower the $P(\theta_r)$ peak is. It shows that under a certain collision energy, the higher the rotational excitation is, the weaker the product rotational angular momentum vector is, which aligns along the direction perpendicular to the relative velocity direction. Furthermore, under a constant rotational quantum number, a higher peak value of $P(\theta_r)$ distribution is obtained at a bigger collision energy, which shows that the alignment of the product rotational angular momentum vector becomes increasingly stronger with the increase of collision energy. The dependences of the $P(\theta_r)$ distribution on collision energy are displayed in Figs. 5(a)–5(e) for the vibrational ground state and four different rotational quantum states on the PES, respectively, which also confirms the abovementioned ordering. For the vibrational ground state and a constant rotational quantum state on the PES, except for the case of $v = 0$ and $j = 5$ at lower collision energy (less than 40 kcal·mol^{-1}) (Fig. 5(c)), a higher peak value of $P(\theta_r)$ distribution can be obtained with a bigger collision energy; for the case of $v = 0$ and $j = 10$ (Fig. 5(d)), the peak of $P(\theta_r)$ distribution disappears and the alignment of the product rotational angular momentum vector becomes the weakest among the four cases.

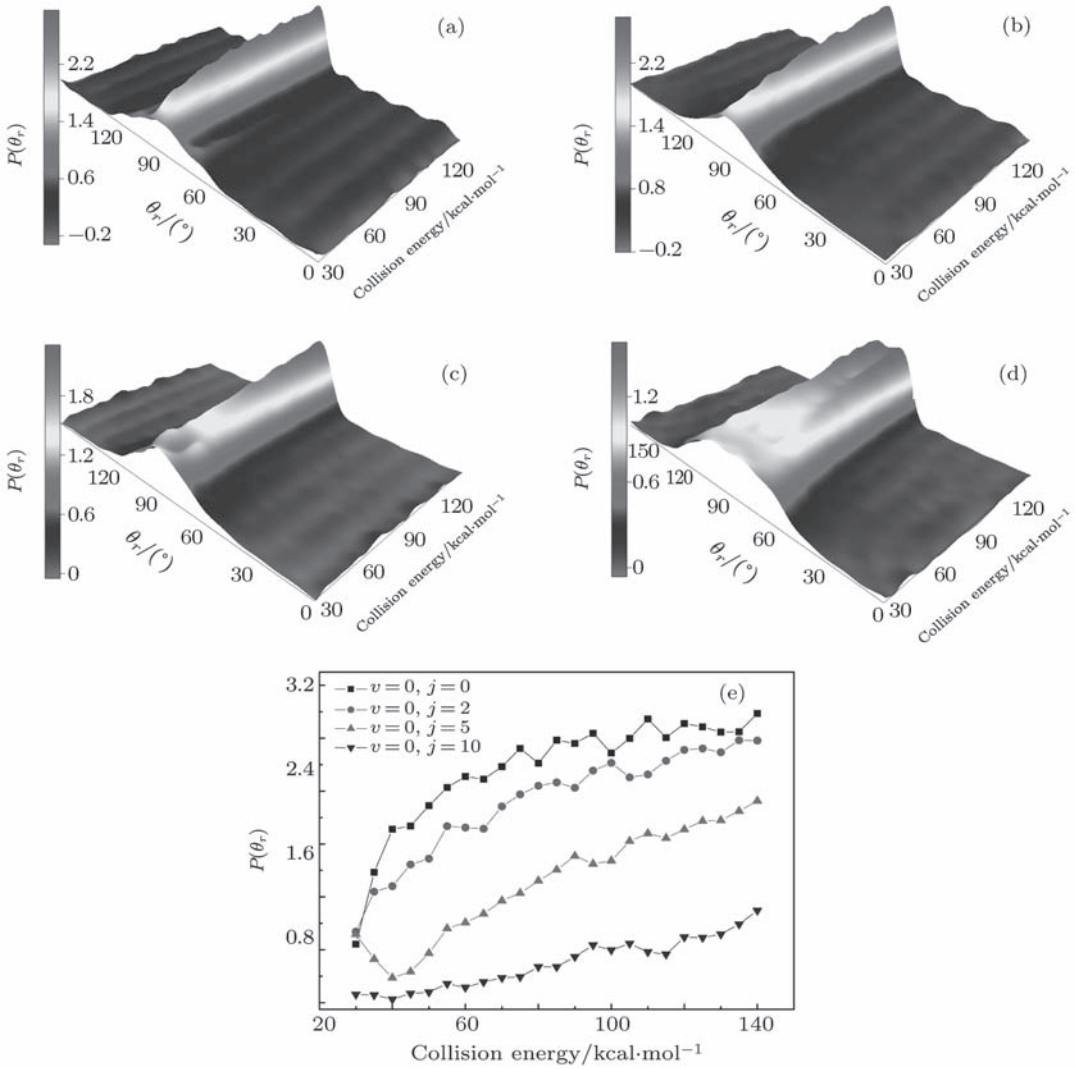


Fig. 5. QCT $P(\theta_r)$ distributions each as a function of the polar angle θ_r and collision energy ($E_c = 30$ kcal·mol^{-1}–140 kcal·mol^{-1}) for the title reactions with (a) $v = 0$ and $j = 0$, (b) $v = 0$ and $j = 2$, (c) $v = 0$ and $j = 5$, (d) $v = 0$ and $j = 10$, and (e) the values of peak at $\theta_r = 90^\circ$ versus collision energy.

The calculated distributions of $P(\phi_r)$ for three collision energies (E_c = 35, 75 and 115 kcal·mol^{-1}) on the PES are shown in Figs. 6(a)–6(c), respectively, describing the $\boldsymbol{k}$–$\boldsymbol{k}'$–$\boldsymbol{j}'$ correlations, in which the $\boldsymbol{k}$–$\boldsymbol{k}'$ scattering plane is at ϕ_r of about 180°, i.e., $\phi_r \approx 180°$. Apparently, the function $P(\phi_r)$ is asymmetric with respect to the scattering plane. The peak or the centre of maximum value of $P(\phi_r)$ appears near $\phi_r = 270°$, which indicates that the rotational angular momentum vector $\boldsymbol{j}'$ of the product NH is oriented mainly along the negative direction of y axis in the centre-of-mass frame. Figure 6(a) shows the $P(\phi_r)$ distributions at a lower collision energy (E_c = 35 kcal·mol^{-1}); from the peak positions of the $P(\phi_r)$ with different rotational quantum number values, it is found that the $P(\phi_r)$ decreases rapidly with the increase of the value of rotational quantum number, which implies that the orientation of the $\boldsymbol{j}'$ depends sensitively on the rotational quantum number. When the collision energy increases (E_c = 75 kcal·mol^{-1} in Fig. 6(b)), the $P(\phi_r)$ distribution is only weakly affected by the rotational excitation of the reactant; as it continues to increase (E_c = 115 kcal·mol^{-1} in Fig. 6(c)), the influence of the rotational excitation of the reactants on $P(\phi_r)$ distribution disappears. The results demonstrate that the orientation of the $\boldsymbol{j}'$ depends sensitively on the collision energy and the rotational quantum number. For clarity, in Figs. 7(a)–7(d), the dependences of the $P(\phi_r)$ distributions on collision energy are displayed for the vibrational ground state and four different rotational quantum states on the PES, respectively. As a further method to study the orientation degree of the rotational angular momentum vector $\boldsymbol{j}'$, figure 7(e) shows the relationships between collision energy and peak value of $P(\phi_r)$ distribution at $\phi_r = 270°$. For the same reactant rotational state, one interesting trend can be obtained from Figs. 7(a)–7(e), i.e., the peak values of $P(\phi_r)$ increase with the increase of the collision energy, and start to decrease after arriving at a maximum value. The product rotational polarizations derived from lower collision energies differ from each other significantly, and the higher the value of j is, the weaker the orientation of rotational angular momentum vector $\boldsymbol{j}'$ is. Although the energy is increased by more than 115 kcal·mol^{-1}, the product rotational polarization keeps basically the same for each of all the reactant rotational states, and the peak of $P(\phi_r)$ distribution flattens and has an about 40° broadband ($\Delta\phi_r \approx 250°$–$290°$). The findings indicate that the abstraction reaction is dominated by out-of-plane mechanisms at a higher collision energy and in a rotational excitation state of the reactant.

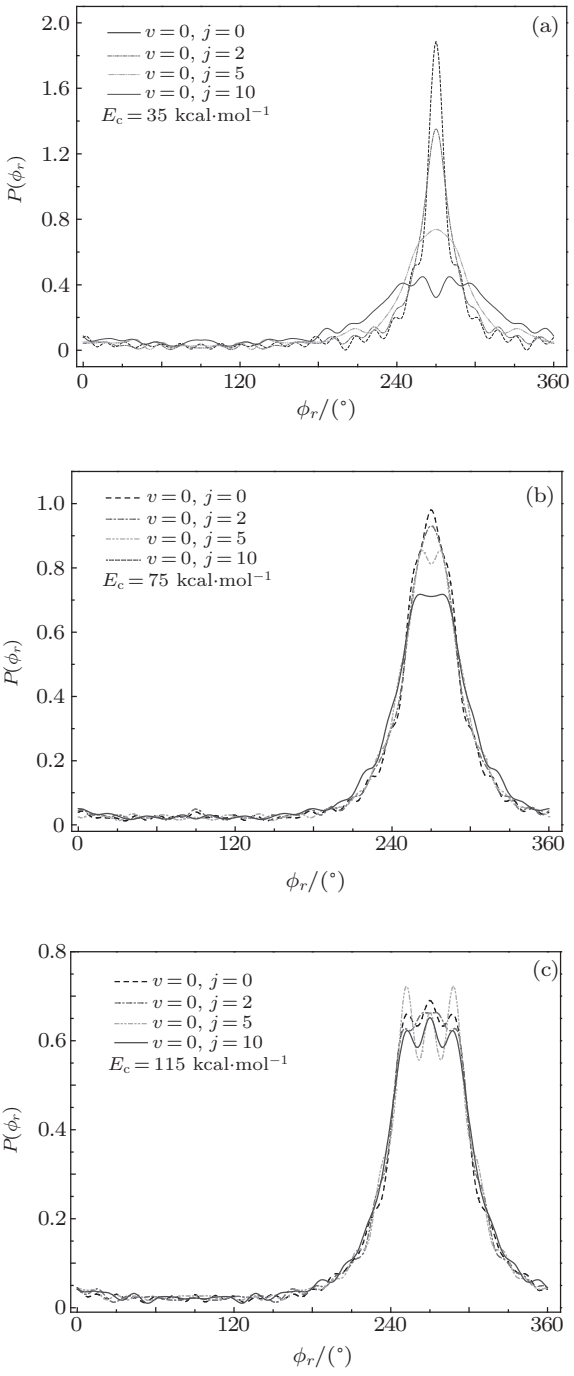


Fig. 6. Angular distributions of $P(\phi_r)$ on the PES at three collision energies describing the $\boldsymbol{k}$–$\boldsymbol{k}'$–$\boldsymbol{j}'$ correlation: E_c = 35 kcal·mol^{-1} (a), 75 kcal·mol^{-1} (b), and 115 kcal·mol^{-1} (c).

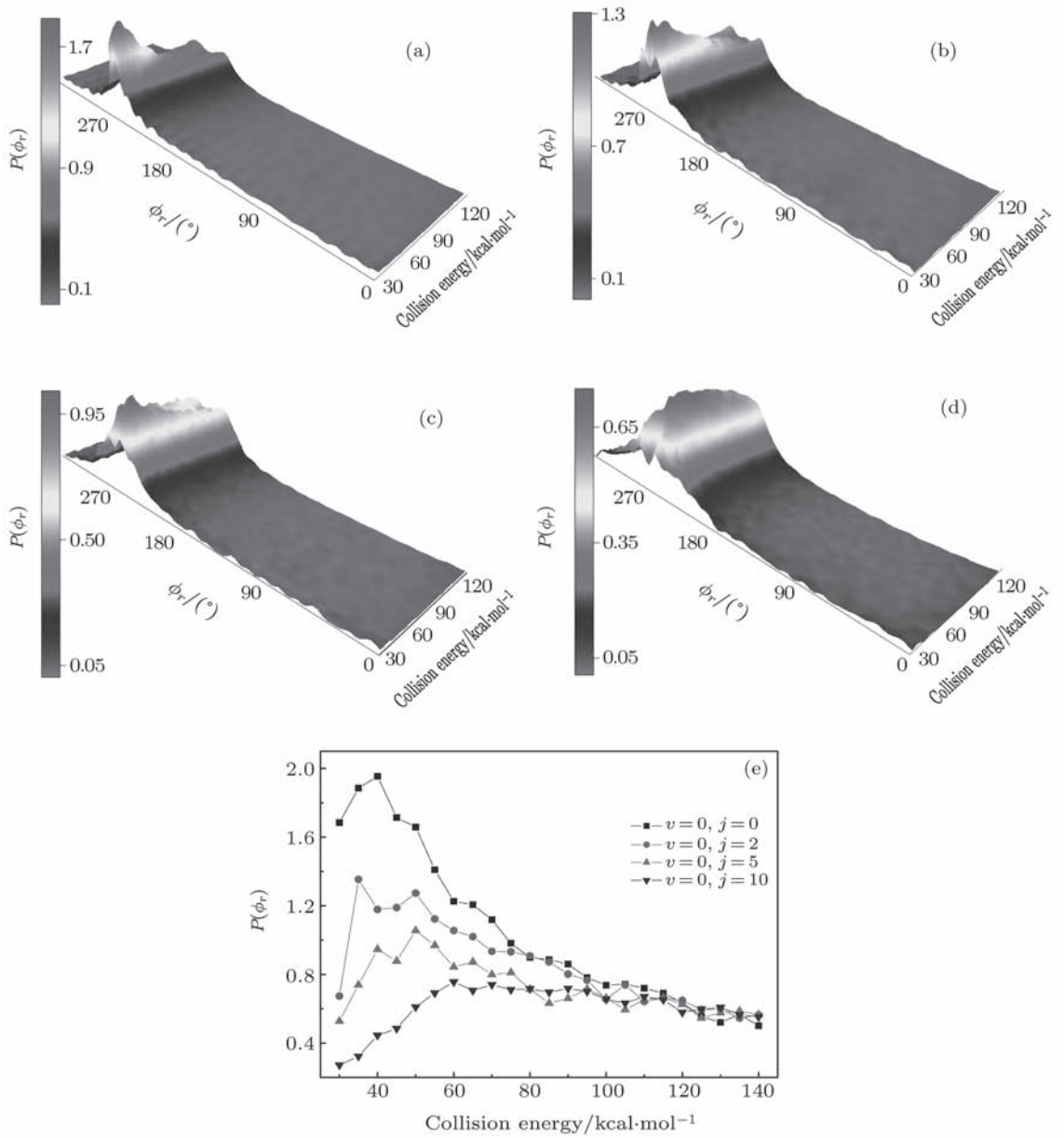


Fig. 7. QCT $P(\phi_r)$ distributions each as a function of the polar angle ϕ_r and collision energy (E_c = 30 kcal·mol^{-1}–140 kcal·mol^{-1}) for the title reactions with (a) $v = 0$ and $j = 0$, (b)$v = 0$ and $j = 2$, (c) $v = 0$ and $j = 5$, (d) $v = 0$ and $j = 10$, and (e) the values of peak at $\phi_r = 270°$ versus collision energy.

In order to validate more information about the angular momentum polarizations, we plot them in the form of polar plots θ_r and ϕ_r averaged over all scattering angles at three collision energies, i.e., E_c = 35 kcal·mol^{-1} with $v = 0$ and $j = 0$ in Fig. 8(a), $v = 0$ and $j = 2$ in Fig. 8(b), and $v = 0$, $j = 5$ in Fig. 8(c); $v = 0$ and $j = 10$ in Fig. 8(d); E_c=75 kcal·mol^{-1} with $v = 0$ and $j = 0$ in Fig. 8(e), $v = 0$ and $j = 2$ in Fig. 8(f), $v = 0$ and $j = 5$ in Fig. 8(g), $v = 0$ and $j = 10$ in Fig. 8(h); E_c = 115 kcal·mol^{-1} with $v = 0$ and $j = 0$ in Fig. 8(i), $v = 0$ and $j = 2$ in Fig. 8(j), $v = 0$ and $j = 5$ in Fig. 8(k), $v = 0$ and $j = 10$ in Fig. 8(l), each of which represents the scattering angle average of the full distribution $P(\theta_r, \phi_r)$. Clearly, the $P(\theta_r, \phi_r)$ distributions peaked at (90°, 270°) for the NH product from the title reaction are in good accordance with the $P(\theta_r)$ distribution and the $P(\phi_r)$ distribution of the products at the collision energies of 35, 75, and 115 kcal·mol^{-1} aforementioned. From the $P(\theta_r, \phi_r)$ distributions, it can be observed that $\boldsymbol{j}'$ is oriented preferentially along the negative direction of the y axis in the rotational ground state and all the excitation states. The $P(\theta_r, \phi_r)$ distributions indicate that the NH is strongly polarized in the direction perpendicular to the scattering plane and rotates mainly in the plane parallel to the scattering plane for all collision energies.

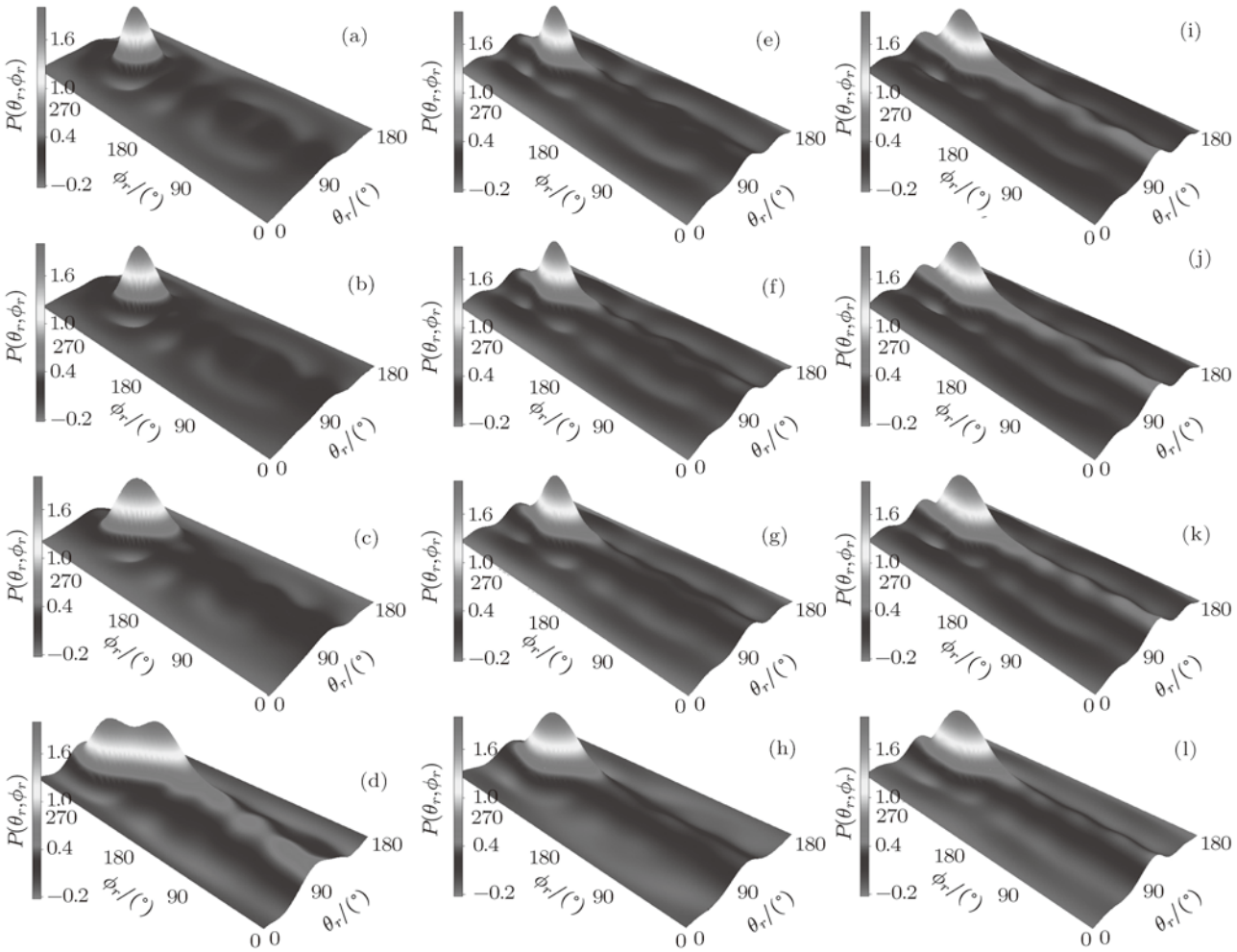


Fig. 8. Polar plots of $P(\theta_r, \phi_r)$ distributions of reactions $N(^4S) + H_2$ ($v = 0$, $j = 0$, 2, 5, 10) → $NH(X^3\Sigma^-) + H$, averaged over all scattering angles at three different collision energies: (a) E_c =35 kcal·mol^{-1}, $v = 0$ and $j = 0$; (b) E_c=35 kcal·mol^{-1}, $v = 0$ and $j = 2$; (c) E_c=35 kcal·mol^{-1}, $v = 0$ and $j = 5$; (d) E_c = 35 kcal·mol^{-1}, $v = 0$ and $j = 10$; (e) E_c=75 kcal·mol^{-1}, $v = 0$ and $j = 0$; (f) E_c=75 kcal·mol^{-1}, $v = 0$ and $j = 2$; (g) E_c=75 kcal·mol^{-1}, $v = 0$ and $j = 5$; (h) E_c=75 kcal·mol^{-1}, $v = 0$ and $j = 10$; (i) E_c=115 kcal·mol^{-1}, $v = 0$ and $j = 0$; (j) E_c=115 kcal·mol^{-1}, $v = 0$ and $j = 2$; (k) E_c=115 kcal·mol^{-1}, $v = 0$ and $j = 5$; (l) E_c=115 kcal·mol^{-1}; $v = 0$ and $j = 10$.

The dependences of the product rotational alignment on collision energy are shown in Fig. 9. It can be seen from Fig. 9 that the $P_2(\cos\theta_r)$ values decrease oscillatorily with the increase of the collision energy at $j = 0$, 2, 5, and 10. It is universally received that for this product alignment parameter, there exists a classical limiting value of −0.5, and the more the value of this parameter approaches to −0.5, the more the product is aligned along the direction perpendicular to $\boldsymbol{k}$. Under a constant rotational quantum number, the curve tendency observed from Fig. 9 thus indicates that the title reaction exhibits stronger product alignment perpendicular to $\boldsymbol{k}$ as the collision energy increases, and it is in accordance with the previous predictions from Figs. 4 and 5. It can also be seen in Fig. 9 that the influence of j on $P_2(\cos\theta_r)$ is not obvious, which is slightly different from the ones shown in Figs. 4 and 5. The reason for it is the difference between $P(\theta_r)$ and $P_2(\cos\theta_r)$ expressions as shown in Eqs. (2) and (4), respectively.

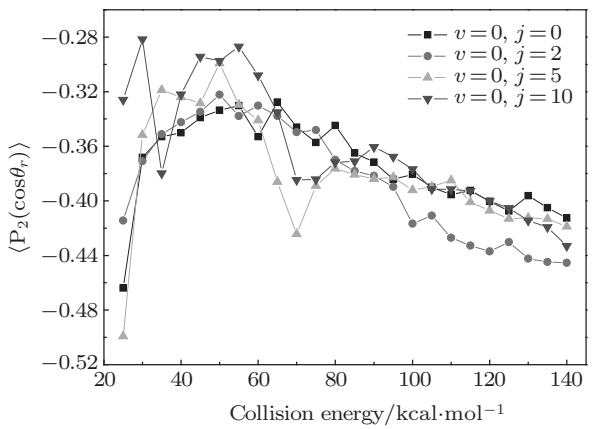


Fig. 9. NH rotational alignment parameter $\langle P_2(\cos\theta_r)\rangle$ values for the reactions $N(^4S) + H_2$ ($v = 0$, $j = 0$, 2, 5, 10) → $NH(X^3\Sigma^-) + H$, each as a function of collision energy.

The differential cross section (DCS) provides the most detailed information about the reaction dynamics and describes only the $\boldsymbol{k}$–$\boldsymbol{k}'$ correlation or the scattering direction of the product. The DCSs for N(^{4}S) + H_2 ($v = 0$, $j = 0$, 2, 5, 10) → NH($X^3\Sigma^-$) + H at $E_c = 35$ kcal·mol^{-1}, plotted each as a function of scattering angle, are shown in Fig. 10. At a low collision energy (35 kcal·mol^{-1}), the DCS shows backward distribution. By comparison with the case of rotational ground state, the DCS is not affected obviously by the lower rotational quantum number reactants ($j = 2$, 5) but closely related to the higher rotational quantum number of reactants ($j = 10$). As a function of both scattering angle θ_t and collision energy, the DCSs for the title reactions are shown in Fig. 11, decomposed into initial rotational states of H_2 with (a) $v = 0$ and $j = 0$, (b) $v = 0$ and $j = 2$, (c) $v = 0$ and $j = 5$, and (d) $v = 0$ and $j = 10$. The angular distributions shift toward the lateral direction with the increase of the collision energy, however, the rotational ground state and the lower rotational excited states of the reactants ($j = 0$, 2, 5) become weaker, while the higher rotational state of the reactants ($j = 10$) is remarkable in the lateral scattering direction of the NH product. This phenomenon of DCS can be ascribed to the contribution of the abstraction reaction.

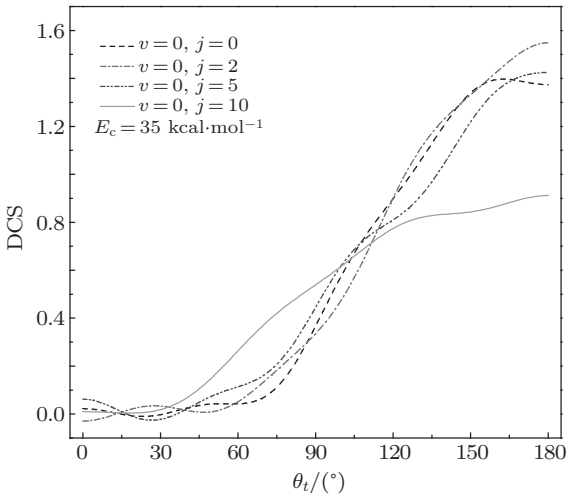


Fig. 10. Differential cross-sections for the reactions N(^{4}S) + H_2 ($v = 0$, $j = 0$, 2, 5, 10) → NH($X^3\Sigma^-$) + H at $E_c = 35$ kcal·mol^{-1} each as a function of scattering angle.

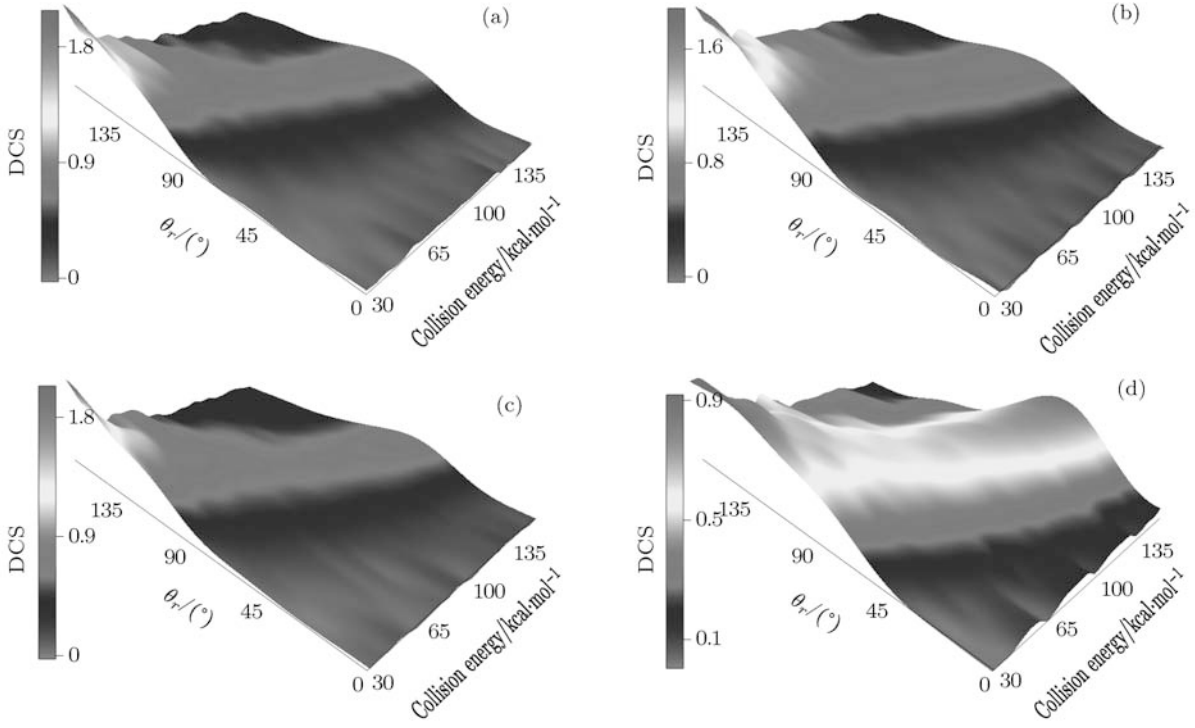


Fig. 11. Differential cross sections each as a function of both scattering angle θ_t and collision energy for reactions N(^{4}S) + H_2 ($v = 0$, $j = 0$, 2, 5, 10) → NH($X^3\Sigma^-$) + H decomposed into initial rotational states of H_2 with (a) $v = 0$ and $j = 0$; (b) $v = 0$ and $j = 2$; (c) $v = 0$ and $j = 5$; (d) $v = 0$ and $j = 10$.

4. Conclusion

In this paper, we present a quasi-classical trajectory study on the product polarizations for the reactions N(^{4}S) + H_2 ($v = 0$, $j = 0$, 2, 5, 10) → NH($X^3\Sigma^-$) + H and stereo dynamic properties at collision energies of 25 kcal·mol^{-1}–140 kcal·mol^{-1}. The distributions of $P(\theta_r)$, $P(\phi_r)$, $P(\theta_r, \phi_r)$, $\langle P_2(\cos\theta_r)\rangle$,

and DCS are calculated with rotational ground state and three different rotational excited states. Results show that the rotational polarizations of the product present different characteristics for both different collision energies and different rotational excited states of the reactants. The distribution of $P(\theta_r)$ demonstrates that the product rotational angular momentum vector $\boldsymbol{j}'$ of the product for the title reaction is strongly aligned in the direction perpendicular to the relative velocity direction $\boldsymbol{k}$, and the product rotational alignment is sensitive to rotational quantum number and collision energy. The distributions of $P(\phi_r)$ and $P(\theta_r, \phi_r)$ show that the product rotational angular momentum vector $\boldsymbol{j}'$ is oriented along the negative direction of y axis of the CM frame. Furthermore, the $\mathrm{P}_2(\cos\theta_r)$ indicates that the product rotational alignment becomes stronger as the collision energy increases. The DCS also predicts that at lower collision energies of the reactants, the scatterings of the product NH are in the backward direction, but they are in lateral direction at higher collision energies; the higher rotational state of the reactants ($j = 10$) is remarkable in the lateral scattering direction of the NH product.

References

[1] Strobel D F 1983 *Int. Rev. Phys. Chem.* **3** 145

[2] Wilson E H and Atreya S K 2004 *J. Geophys. Res.* **109** E06002

[3] Prasad K, Yetter R A and Smooke M D 1997 *Combust. Sci. Technol.* **124** 35

[4] Umemoto H, Asai T and Kimura Y 1997 *J. Chem. Phys.* **106** 4985

[5] Chu T S, Han K L and Varandas A J C 2006 *J. Phys. Chem.* A **110** 1666

[6] Balucani N, Alagia M, Cartechini L, Casavecchia P, Volpi G G, Pederson L and Schatz G C 2001 *J. Phys. Chem.* A **105** 2414

[7] Honvault P and Launay J M 1999 *J. Chem. Phys.* **111** 6665

[8] Pederson L A, Schatz G C, Ho T S, Hollebeek T, Rabitz H, Harding L B and Lendvay G 1999 *J. Chem. Phys.* **110** 9091

[9] Koshi M, Yoshimura M, Fukuda K, Matsui H, Saito K, Watanabe M, Imamura A and Chen C 1990 *J. Chem. Phys.* **93** 8703

[10] Takayanagi T, Kurosaki Y and Yokoyama K 2000 *Chem. Phys. Lett.* **321** 106

[11] Zhang S W and Thanh N T 2000 *J. Chem. Phys.* **113** 6149

[12] Pascual R Z, Schatz G C, Lendvay G and Troya D 2002 *J. Phys. Chem.* A **106** 4125

[13] Davidson D F and Hanson R K 1990 *Int. J. Chem. Kinet.* **22** 843

[14] Poveda L A and Varandas A J C 2005 *Phys. Chem. Chem. Phys.* **7** 2867

[15] Werner H J and Knowles P J 1988 *J. Chem. Phys.* **89** 5803

[16] Knowles P J and Werner H J 1988 *Chem. Phys. Lett.* **145** 514

[17] Varandas A J C 1988 *Adv. Chem. Phys.* **74** 255

[18] Han B R, Yang H, Zheng Y J and Varandas A J C 2010 *Chem. Phys. Lett.* **493** 225

[19] Adam L, Hack W, Zhu H, Qu Z W and Schinke R 2005 *J. Chem. Phys.* **122** 114301

[20] Carmona-Novillo E, Gonzalez-Lezana T, Roncero O, Honvault P, Launay J M, Bulut N, Aoiz F J, Banares L, Trottier A and Wrede E 2008 *J. Chem. Phys.* **128** 15

[21] Wang M L, Han K L and He G Z 1998 *J. Phys. Chem.* A **102** 10204

[22] Zhang W Q, Cong S L, Zhang C H, Xu X S and Chen M D 2009 *J. Phys. Chem.* A **113** 4192

[23] Zhao J, Xu Y and Meng Q T 2010 *Chin. Phys.* B **19** 063403

[24] Zhu T, Hu G D, Chen J Z, Liu X G and Zhang Q G 2010 *Chin. Phys.* B **19** 083402

[25] Zhao J and Luo Y 2011 *Chin. Phys.* B **20** 043402

[26] Xu Z H and Zong F J 2011 *Chin. Phys.* B **20** 063104

[27] Li R J, Han K L, Li F E, Lu R C, He G Z and Lou N Q 1994 *Chem. Phys. Lett.* **220** 281

[28] Chu T S 2010 *J. Comput. Chem.* **31** 1385

[29] Mcclelland G M and Herschbach D R 1979 *J. Phys. Chem.* A **83** 1445

[30] Barnwell J D, Loeser J G and Herschbach D R 1983 *J. Phys. Chem.* A **87** 2781

[31] Wang M L, Han K L and He G Z 1998 *J. Chem. Phys.* **109** 5446

[32] Shaferray N E, Orrewing A J and Zare R N 1995 *J. Phys. Chem.* **99** 7591

[33] Brouard M, Lambert H M, Rayner S P and Simons J P 1996 *Mol. Phys.* **89** 403

[34] Han K L, He G Z and Lou N Q 1996 *J. Chem. Phys.* **105** 8699

[35] Chen M D, Han K L and Lou N Q 2002 *Chem. Phys. Lett.* **357** 483

[36] Chen M D, Han K L and Lou N Q 2003 *J. Chem. Phys.* **118** 4463

[37] Ma J J, Chen M D, Cong S L and Han K L 2006 *Chem. Phys.* **327** 529

[38] Han B R, Zong F J, Wang C L, Ma W Y and Zhou J H 2010 *Chem. Phys.* **374** 94

[39] Ju L P, Han K L and Zhang J Z H 2009 *J. Comput. Chem.* **30** 305

[40] Xu Y, Zhao J, Yue D G, Liu H, Zheng X Y and Meng Q T 2009 *Chin. Phys.* B **18** 5308

[41] Chu T S, Zhang Y and Han K L 2006 *Int. Rev. Phys. Chem.* **25** 201